Cancer Letters 501 (2021) 224–233

Contents lists available at ScienceDirect

Cancer Letters

journal homepage: www.elsevier.com/locate/canlet

DIO3, the thyroid hormone inactivating enzyme, promotes tumorigenesis and metabolic reprogramming in high grade serous ovarian cancer

Dotan Moskovich [a,b], Adi Alfandari [a,b], Yael Finkelshtein [a,b], Avivit Weisz [d,e], Aviva Katzav [d,e], Debora Kidron [c,d,e], Evgeny Edelstein [d,e], Daniel Veroslavski [f], Ruth Perets [f], Nissim Arbib [c,g], Yfat Kadan [g], Ami Fishman [c,g], Bernard Lerer [h], Martin Ellis [a,c], Osnat Ashur-Fabian [a,b,*]

[a] Translational Oncology Laboratory, Hematology Institute and Blood Bank, Meir Medical Center, Kfar-Saba, Israel
[b] Department of Human Molecular Genetics and Biochemistry, Sackler School of Medicine, Tel Aviv University, Tel Aviv, Israel
[c] Sackler School of Medicine, Tel Aviv University, Tel Aviv, Israel
[d] Department of Pathology, Meir Medical Center, Kfar Saba, Israel
[e] Sackler Faculty of Medicine, Israel
[f] Clinical Research Institute at Rambam, Division of Oncology, Rambam Health Care Campus, Technion-Israel Institute of Technology, Haifa, Israel
[g] Gynecological Oncology Unit, The Department of Obstetrics and Gynecology, Meir Medical Center, Kfar Saba, Israel
[h] Biological Psychiatry Laboratory Hadassah - Hebrew University Medical Center, Jerusalem, Israel

ARTICLE INFO

Keywords:
Deiodinases
Thyroid hormones
Gynecological malignancy
Ovarian cancer
Metabolism

ABSTRACT

High grade serous ovarian cancer (HGSOC) is the most lethal gynecologic malignancy with a need for better understanding the disease pathogenesis. The biologically active thyroid hormone, T3, is considered a tumor suppressor by promoting cell differentiation and mitochondrial respiration. Tumors evolved a strategy to avoid these anticancer actions by expressing the T3 catabolizing enzyme, Deiodinase type 3 (DIO3). This stimulates cancer proliferation and aerobic glycolysis (Warburg effect). We identified DIO3 expression in HGSOC cell lines, tumor tissues from mice and human patients, fallopian tube (FT) premalignant lesion and secretory cells of normal FT, considered the disease site-of-origin. Stable DIO3 knockdown (DIO3-KD) in HGSOC cells led to increased T3 bioavailability and demonstrated induced apoptosis and attenuated proliferation, migration, colony formation, oncogenic signaling, Warburg effect and tumor growth in mice. Proteomics analysis further indicated alterations in an array of cancer-relevant proteins, the majority of which are involved in tumor suppression and metabolism. Collectively this study establishes the functional role of DIO3 in facilitating tumorigenesis and metabolic reprogramming, and proposes this enzyme as a promising target for inhibition in HGSOC.

1. Introduction

High grade serous ovarian cancer (HGSOC) is a gynecological malignancy associated with excessively large number of deaths, due to late diagnosis after the disease has metastasized to distant sites [1]. Recent studies strongly suggest that secretory cells of the distal fallopian tube (FT) epithelium are the source of HGSOC, rather than the ovarian surface as previously believed [2,3]. The first step in FT secretory cells transformation to HGSOC is a mutation in the tumor suppressor gene p53, also known as p53 signature. By accumulation of additional mutations, a premalignant serous tubal intraepithelial carcinoma (STIC) lesion is developed and later implants on the ovary, resulting in the primary tumor [2]. Identifying new players could lead to improved understanding of disease pathogenesis and novel therapeutic targets.

Cancer is characterized by continuous proliferation which relies on the Warburg effect, the production of energy mainly through aerobic glycolysis rather than mitochondrial respiration [4]. For this reason, the biologically active thyroid hormone, 3,5,3′-triiodo-L-thyronine (T3) which regulates cell differentiation and mitochondrial respiration via binding to nuclear thyroid receptor, is considered a tumor suppressor [5]. Accordingly, various tumors have evolved a strategy of avoiding these anti-cancer activities by expressing the T3-catabolizing membranal enzyme, deiodinases type 3 (DIO3), which degrades T3 before it can reach the nuclear receptors [6–8]. This provides dynamic changes in intracellular T3 levels and contributes to processes involved in cancer progression.

* Corresponding author. Translational Oncology Laboratory, Hematology Institute and Blood Bank, Meir Medical Center, Kfar-Saba, 44821, Israel.
E-mail address: osnataf@gmail.com (O. Ashur-Fabian).

https://doi.org/10.1016/j.canlet.2020.11.011
Received 13 August 2020; Received in revised form 18 October 2020; Accepted 11 November 2020
Available online 19 November 2020

DIO3 upregulation was shown to be controlled by multiple oncogenic signaling pathways [6]. This, together with the fact that DIO3 is highly expressed during fetal development, less frequent in most healthy adult tissues and is reexpressed in cancer tissues, suggests an oncofetal nature for this enzyme. In contrast, the other deiodinase family members, DIO1 and DIO2, which are mainly responsible for the activation of T3 from the pro-hormone T4, were reported to be downregulated is several cancer models [9]. Although DIO3 emerged as a new player in cancer, its function was studied in few cancer models [10–14] but not in ovarian cancer. In this current work, we identified DIO3 expression in HGSOC and provided evidence for the involvement of this unique enzyme in disease progression.

2. Materials and methods

2.1. Antibodies

All primary antibodies are detailed in Supplementary Table 1.

2.2. Cell cultures

HGSOC (OVCAR3, KURAMOCHI and JHOS4) and FT's cells (FT237 and FT282) were provided by Dr. Ruth Perets (Rambam Medical Center, Haifa, Israel). The non HGSOC control cell line, A2780, was obtained from Sigma Aldrich (St. Louis, MO, USA). Chinese hamster normal ovary cells (CHO–K1) were a kind gift from Prof. Philippe Clézardin (University of Lyon, Lyon, France). OVCAR3, KURAMOCHI, A2780 and CHO–K1 were grown in RPMI1640 medium, JHOS4 and FT's were grown in DMEM F-12 medium (Biological Industries, Beit Haemek, Israel). All cells are supplemented with 10% heat-inactivated FBS and 1% penicillin-streptomycin antibiotics. For T3 deficient medium, the cells were grown in 10% charcoal stripped serum, containing depleted levels of thyroid hormones (Biological Industries). T3 was purchased from Sigma Aldrich. STR/mutation profiling was used for authentication and mycoplasma was screened periodically.

2.3. Human tissue samples

Tumor tissues were collected from 10 HGSOC patients at diagnosis undergoing primary debulking surgery as well as normal ovarian and FT fimbria tissues from 8 non-oncological patients undergoing laparotomy or ultrasound guided paracentesis treated at the Obstetrics and Gynecology Department, Meir Medical Center, Israel. HGSOC diagnosis was confirmed based on clinical and pathological characteristics. The tissues were formalin-fixed-paraffin-embedded (FFPE) and 4 μm sections were cut from the tissue blocks at the Meir Medical Center Pathology Department. Tissues were collected upon informed consent, in compliance with Institutional Review Board approval, in accordance with the Declaration of Helsinki.

2.4. Tissues from ovarian cancer mouse model

This model uses the PAX8 promoter, a Müllerian marker which is positive in FT secretory cells, to drive deletion of BRCA1 or BRCA2, P53 and PTEN. As a result the mice develop tumors that are indistinguishable from the HGSOC human disease [15]. Tumor FFPE section slides were obtained from Dr. Ruth Perets (Rambam Medical Center, Haifa, Israel). This study was approved by the Israeli animal ethics committee (approval number IL-064-05-2017).

2.5. Western blots (WB)

Total proteins were extracted and separated on 10–12.5% polyacrylamide gels, fast-transferred to PVDF membranes and analyzed by Western blot using specific primary antibodies. Bound antibodies were visualized using horseradish peroxidase (HRP)-conjugated secondary antibodies goat anti-Rabbit IgG or goat anti-Mouse IgG (Jackson ImmunoResearch Laboratories, West Grove, PA, USA), followed by enhanced chemiluminescence (ECL) detection kit (PIERCE, Thermo Fisher Scientific, Bremen, Germany). Integrated optical densities (IOD) of the bands was measured by Las3000 imaging system, analyzed by Multi-gauge v3.0 software (Fujifilm Life Science, Tokyo, Japan) and normalized to protein loading using Ponceau S stain and/or β tubulin.

2.6. Immunohistochemistry (IHC)

Staining was done using specific antibodies on a Ventana Benchmark XT automatic stainer (Ventana, Tucson, Arizona, USA). Slides were analyzed by board-certified pathologists.

2.7. Immunofluorescence (IF)

FFPE tissues underwent deparaffinization and antigen retrieval using a Ventana Benchmark XT automatic stainer. Next, the tissues were manually blocked with 3% BSA and incubated overnight at 4 °C with antibodies against DIO3 and PAX8. The day after, slides were washed 3 times with PBS (Mg^{2+}, Ca^{2+})-Triton and labeled green with donkey anti-Rabbit IgG-NL493 and red with donkey anti-Mouse IgG-NL557 (R&D systems, Abingdon, UK). Nucleus was stained blue with Hoechst (33342, molecular probes, Eugene, OR, USA).

2.8. Microscopy

Images were obtained by a microscope equipped with a camera with Olympus model BX41 for IHC and IF slides and model IX71 for cell cultures (Olympus, Tokyo, Japan). Analysis was performed by cellSens Entry Olympus imaging software.

2.9. DIO3 knockdown (DIO3-KD) HGSOC cells

OVCAR3 cells were seeded (0.5×10^6/6 well plates) and stably transfected with a pool of 3 human DIO3 shRNA plasmids (Cat. # sc-77150-SH) or a nonspecific scrambled control shRNA plasmids (Cat. # sc-108060), from Santa Cruz Technologies (Dallas, TX, USA). Transfections were performed following manufacturer's instructions with shRNA transfection reagent (Cat. # sc108061, Santa Cruz). After selection with puromycin and clones isolation, successful stable inhibition was confirmed at the RNA (Real-time PCR) and protein levels (Western blots).

2.10. Real-time PCR

Real-Time PCR (7500 Fast system) and Fast Sybr Green Master Mix were used (Applied Biosystems, Carlsbad, CA, USA). Fold change was calculated using the comparative threshold cycle method (2-ΔΔCT) relative to control cells. Primers (Hylabs, Rehovot, Israel) for DIO3 and β-actin (for normalization) were: β-actin forward primer: 5′-CCTGGCACCCAGCACAAT-3'. Reverse primer: 5′-GCCGATCCACACGGAGTACT-3'. DIO3 forward primer: 5′-GCCTACTTCGAGCGTCTCTATG-3'. Reverse primer: 5′-CATAGCGTTC CAACCAAGTGCG-3'.

2.11. Flow cytometry (FC)

Absolute cell counts, cell cycle and Annexin V/Propidium Iodide (Annexin-PI) were performed using MACSQuant flow cytometer (Miltenyi Biotec, Bergisch Gladbach, Germany), as detailed before [16,17]. For DIO3 expression cells were permeabilized and labeled with a fluorescently-conjugated DIO3 antibody.

2.12. Soft agar colony assay

OVCAR3 and DIO3-KD OVCAR3 cells were resuspended in 0.6%

noble agar (A5431, Sigma Aldrich) in growth medium, and plated onto a solid layer of 0.9% noble agar in growth medium in 6-well plates in four independent replicates. Fresh medium was added two times a week for four weeks. Plates were stained with 0.05% crystal violet in 10% Neutral Buffered Formalin overnight and washed. Colonies counts and predefined reference colony size (area>200 pixels) were analyzed using OpenCFU software (http://opencfu.sourceforge.net/).

2.13. Wound healing assay

IncuCyte ZOOM™ real time live cell imaging system (Essen BioScience, MI USA) was used to calculate the relative wound density within the initially-vacant area at each time point.

2.14. HGSOC xenograft model

9 weeks old female athymic nude mice (n = 7, Envigo, Ness-Ziona, Israel) were subcutaneously injected with DIO3-KD OVCAR3 cells and scrambled control OVCAR3 cells (1×10^6 cells each) into the right and left flanks, respectively. Analysis of tumor growth inhibition was examined by volume measurements and excised tumor weight at animal sacrifice. At study end (28 days) xenograft tumors were collected for protein extractions or FFPE preparations and evaluated for DIO3 levels. The study was outsourced (Almog Diagnostic LTD, Shoham, Israel) in compliance with the recommendations of the Guide for Care and Use of Laboratory Animals and following Helsinki approval.

2.15. Proteomics analysis

Total proteins were extracted from OVCAR3 and DIO3-KD OVCAR3 cells (duplicates), digested by trypsin and analyzed by LC-MS/MS on Q Exactive™ HF-X Mass Spectrometer (Thermo Fisher Scientific). Proteins were identified by Discoverer software version 1.4 against the Human sequence using the search algorithms Sequest (Thermo Fisher Scientific) and Mascot search engines. Identified peptides were filtered with high confidence, top rank, mass accuracy, and a minimum of 2 peptides. High confidence peptides have passed the 1% false discovery rate (FDR) threshold (estimated false positives in a list of peptides). Semi quantification was done by calculating the peak area of each peptide. Keratins were filtered out since they might be a contamination that origins from dust, hair and skin.

2.16. Protein enrichment analysis and classification

ClustVis web tool (https://biit.cs.ut.ee/clustvis) was used for multivariate cluster analysis using Principal Component Analysis (PCA) and heatmap [18]. Protein classification was performed using the PANTHER tool (http://pantherdb.org) [19]. Protein-protein interaction network was generated using STRING v. 11 (https://string-db.org) [20].

2.17. Statistical analysis

Experiments were repeated independently in duplicates or triplicates and analyzed by two-sided unpaired *t*-test and by ANOVA for multiple comparisons. The animal study was analyzed by a paired *t*-test. Significance was determined at $p < 0.05$. Results are presented as mean ± STE.

2.18. Data availability

Full proteomics datasets are available from the corresponding author upon reasonable request.

3. Results

3.1. DIO3 is expressed in normal fallopian tube and HGSOC cells and composes a stable dimer

We aimed to assess the basal expression of DIO3 in human HGSOC cells. Flow-cytometry results (Supplementary Fig. 1A) indicated that DIO3 is significantly higher in HGSOC (OVCAR3) compared to non-HGSOC cells (A2780) and is lowest in normal ovary cells (CHO–K1). Next, DIO3 protein levels were evaluated by WB in additional HGSOC cells (KURAMOCHI and JHOS4), which, similar to OVCAR3, were reported to highly resemble the genomic profile of the human disease [21]. DIO3 was further examined in cell lines generated from normal FT secretory cells (FT237 and FT282), the cell-of-origin of HGSOC [22]. Results identified two DIO3 bands (Fig. 1A), one at the predicted monomer size (37 kDa) and the second at a higher molecular weight (75 kDa). Quantification of the two bands indicated that compared to normal ovary and the non-HGSOC cells, DIO3 levels were enhanced in the FT and HGSOC cells. The specificity of both bands was validated using blocking peptide that prevents antibody binding to the DIO3 epitope (Supplementary Fig. 1B). As DIO3 gene is composed of a single exon and is active only as a stable homodimer [23,24], we speculated that the higher band represents the dimeric enzyme conformation. This form is known to resist denaturing conditions and is disassembled by high-molar Dithiothreitol (DTT) concentrations [25]. Accordingly, DTT degraded the 75 kDa DIO3 band in HGSOC and FT cells, confirming that these cells mainly express the enzyme active dimeric form (Fig. 1B). By incubating OVCAR3 cells with a translation inhibitor cycloheximide (CHX), we have further demonstrated that the DIO3 dimer is highly stable, persisting for up to 72 h, compared to only 24 h for the enzyme monomer (Fig. 1C). The higher stability of the dimer may be explained by the strong S–S bonds between the monomers, together with essential interactions with phospholipids and other proteins in the membrane [25,26]. Collectively, we provide the first indication for an active DIO3 enzyme in both the cell-of-origin as well as tumor cells of HGSOC.

3.2. DIO3 is expressed in HGSOC tissues throughout tumor evolution

DIO3 expression was next assessed in tumor and normal human tissues (Supplementary Table 2), collected from 10 HGSOC patients (Pt#1–10) and 8 non-oncological patients (N#1–8). We focused on tissues representing the different stages of HGSOC development, including non-neoplastic ovaries and FT's, the premalignant STIC lesion, primary tumors and metastatic sites. All samples underwent IHC analysis for DIO3 expression, parallel to common disease markers [3,27] to confirm tumor regions (Fig. 2A). These included mutated p53, the proliferation marker Ki-67 and nuclear PAX8, a Müllerian marker which is positive in FT secretory cells. Low DIO3 staining was observed in normal ovaries, while secretory cells of normal FT strongly expressed this enzyme. This corresponds with PAX8 staining pattern. DIO3 was highly positive in STIC precursor lesion, as well as in tumor-defined regions of primary and metastatic tissues. This unique DIO3 expression was further confirmed by IF in PAX8 positive secretory cells of normal FT, as well as in STIC and tumor tissues, particularly in the cell membrane (Fig. 2B), corresponding with the well-established localization of the active-dimeric enzyme form [23]. Similar results were obtained in additional normal ovaries (Supplementary Fig. 2A), normal FT tissues (Supplementary Fig. 2B) and HGSOC tissues (Supplementary Fig. 3).

DIO3 expression was further validated in a genetically engineered HGSOC mouse model. Similar to human tissues, we observed a classical membrane expression of DIO3 in PAX8 positive mouse tumor cells (Fig. 2C). For all human and mice samples, negative isotype controls were used (Supplementary Fig. 4). Taken together, our results strongly suggest that the DIO3 enzyme is present throughout the various stages of HGSOC development, signifying potential involvement in disease pathogenesis.

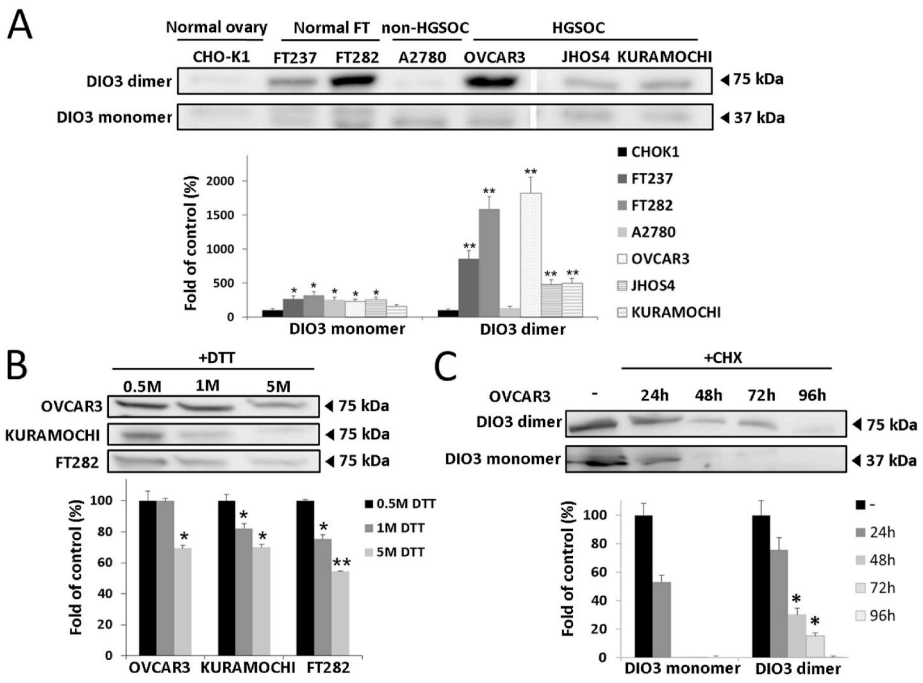

Fig. 1. DIO3 dimer is expressed in FT and HGSOC cells and is highly stable. (A) Normal ovaries and FT cells, HGSOC and non-HGSOC cell lysates were analyzed by WB for DIO3 monomeric and dimeric forms (Upper panel). Skipping lane is clearly marked by a separating line. Quantification of normalized bands intensity, as fold from CHO–K1 (Lower panel). Protein loading is presented in Supplementary Fig. 1C. Values are mean ± STE. *, $p < 0.05$. **, $p < 0.005$ **(B)** OVCAR3, KURAMOCHI and FT282 cell lysates were incubated with 0.5–5 M Dithiothreitol (DTT) and analyzed by WB (Upper panel). Quantification of normalized bands intensity, as fold of 0.5 M DTT (Lower panel). Values are mean ± STE. *, $p < 0.05$. **, $p < 0.005$. Protein loading is presented in Supplementary Fig. 1D **(C)** OVCAR3 cells were seeded (1×10^5/24 well plates) and DIO3 dimer and monomer degradation rates were assessed following a single treatment with 10 μg/ml of the translation inhibitor cycloheximide (CHX) for up to 96 h (Upper panel). Quantification of bands intensity, as fold of control (Lower panel). Values are mean ± STE. *, $p < 0.05$, significance compared to monomeric form.

3.3. DIO3 silencing results in T3-related anti-cancer effects in vitro and tumor growth inhibition in vivo

To study the role played by DIO3 in ovarian tumorigenesis, we generated stable DIO3 knockdown HGSOC cells (DIO3-KD) using specific shRNA plasmids. Mock-transfected cells were used as controls. OVCAR3 HGSOC cells, which exhibited the most profound expression of the active dimeric enzyme, served as the 'proof of concept' model. We established a 50% reduction in DIO3 mRNA (Fig. 3A) and in the monomeric and dimeric protein forms in a single isolated clone (Fig. 3B). As DIO3 role is to catabolize T3, we further examined in the silenced cells μ-crystallin, also known as CRYM. This enzyme is an intracellular T3 binding protein which was shown to blunt T3 activity [28,29] and to be reciprocally inhibited by T3 itself [30]. We observed a significant reduction in this protein (Fig. 3B), suggesting an increase in T3 bioavailability for performing its tumor suppressor activities. In addition, we observed an altered phenotype with significant reduction in cell number and accumulation of apoptotic cell aggregates (Fig. 3C, left panel). We validated that this phenotype is T3-related, as incubating the cells in T3-free medium led to loss of phenotype (Fig. 3C, middle panel), which was rescued upon replenishment with physiological T3 concentrations (Fig. 3C, right panel). These results were confirmed by cell number quantification (Fig. 3D). Cell cycle and Annexin-PI analyses demonstrated that DIO3 silencing initially led to lower mitotic rate with a reduction in S-G2M (Fig. 3E, upper panel) but not cell death (Fig. 3E, lower panel). A few days later significant apoptosis was evident, as demonstrated by induction in Sub-G1 (Fig. 3F, upper panel) and Annexin-PI positivity (Fig. 3F, lower panel). Next, anchorage-independent growth, a hallmark of carcinogenesis, was assessed by soft agar colony formation assay. The DIO3 depleted cells exhibited a 30% reduction in colony formation and 80% reduction in colony size (Fig. 3G). Examining DIO3 role in ovarian cancer cell migration by preforming wound-healing assay indicated attenuated wound healing closure (Fig. 3H, left panel). Quantification of wound density dynamics is presented in Fig. 3H, right panel. After observing that DIO3 silencing results in multiple T3-related anti-cancer effects, we analyzed by WB a collection of proteins involved in oncogenic signaling pathways and glucose metabolism (Fig. 3I). A significant 20–70% decrease was observed in phosphorylated ERK (pERK), PAX8, β-catenin and the phosphorylated p85 regulatory subunit of PI3K (pPI3K p85). This corresponds with the low proliferation rate observed in the DIO3 silenced cells. Notably, the levels of key glycolytic enzymes [31] were similarly reduced. These include the 6-phosphofructokinase platelet type (PFKP), Glyceraldehyde 3-phosphate dehydrogenase (GAPDH) and Pyruvate kinase 2 (PKM2). In parallel, we observed a 30% induction in ATP5 synthase subunit alpha (ATP5A), which belongs to the mitochondrial ATP5 oxidative phosphorylation complex [32]. This suggests a metabolic switch, from aerobic glycolysis (Warburg effect) towards mitochondrial respiration. Collectively, we demonstrate a major role for DIO3 in HGSOC tumorigenesis.

After establishing the involvement of DIO3 in HGSOC *in vitro*, we examined whether DIO3 silencing will affect tumor growth *in vivo*. Nude female mice (n = 7) were subcutaneous inoculated with 1×10^6 control cells (Left flank) or the DIO3-KD cells (Right flank). Volume measurements during the 28 days study period confirmed attenuated tumor growth in the DIO3-KD cells compared to control (Fig. 4A). Inoculated and excised tumors from a representative mouse at study end are shown in Fig. 4B. Results indicate that the average tumor weight was reduced by 35% in the DIO3-KD tumors (Fig. 4C). DIO3 remained silenced throughout the experimental period, as demonstrated by IHC and WB analyses (Fig. 4D). Taken together, the *in vitro* and *in vivo* preclinical studies established a functional role for DIO3 in HGSOC tumor growth.

3.4. Integrative proteomics analysis reveals DIO3-involvement in ovarian tumor growth and metabolism

To fully elucidate the biological function of DIO3 in HGSOC, we aimed to study global proteins altered following DIO3 silencing. Proteomics analysis identified approximately 237 proteins which were significantly distinct between DIO3-KD and control cells. The two cell models demonstrated cluster segregation by heatmap (Fig. 5A) and principal component analysis (Fig. 5B). The altered proteins are involved in two main subcategories of biological processes (Fig. 5C), including metabolism (22%), as well as cellular processes (30%), of which the majority are also metabolism-related (36%). We next focused on 152 proteins with alterations greater than 25% in the DIO3-silenced cells. An interaction network (Fig. 5D) indicates that the majority of these proteins (67%) are associated with metabolism. A highly

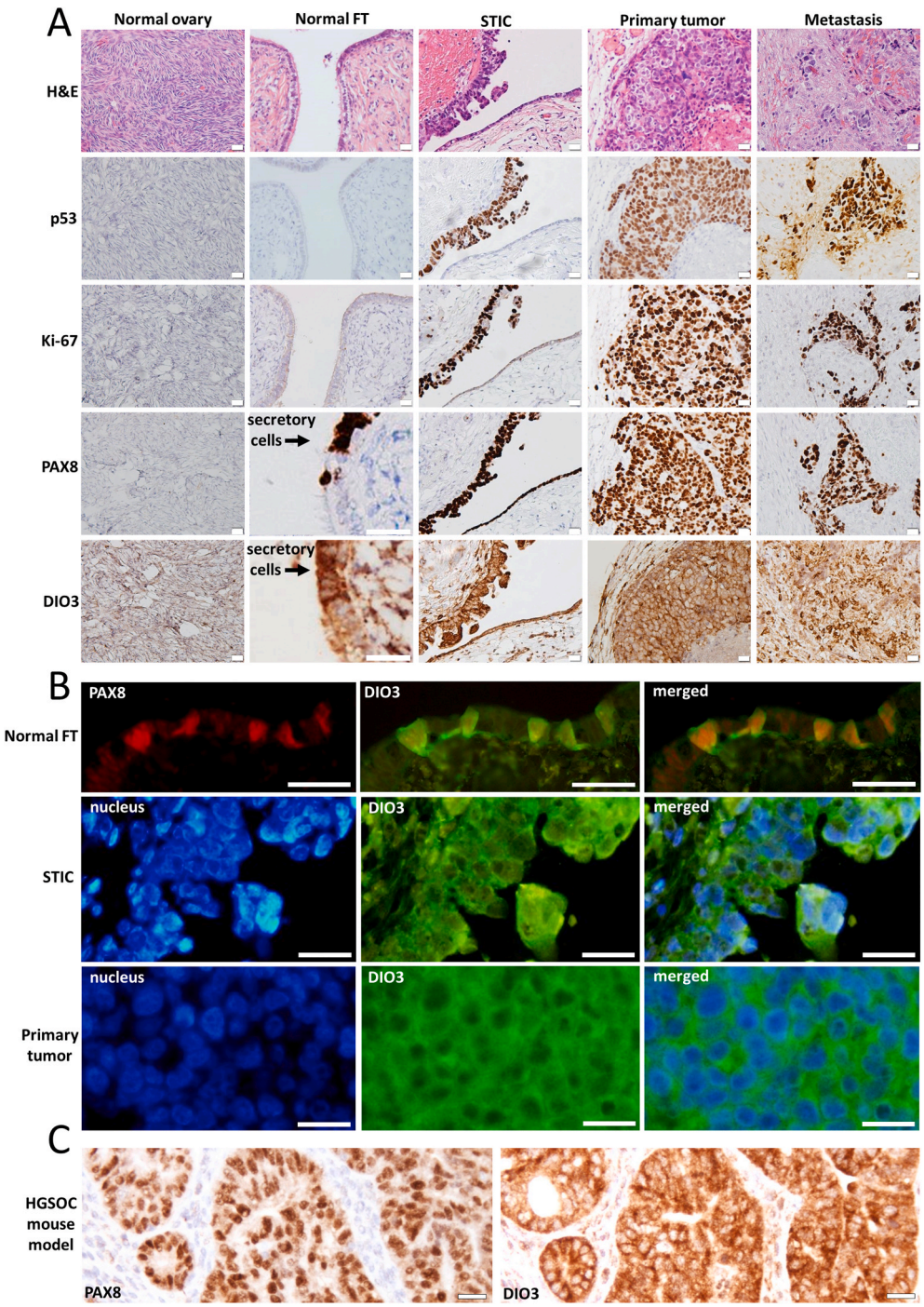

Fig. 2. DIO3 is expressed in normal FT and HGSOC human and mouse tissues. **(A)** IHC staining of p53, Ki-67, PAX8 and DIO3 in representative FPPE tissues of normal ovary and FT epithelium, as well as STIC, primary and colon metastasis from a HGSOC patient. To demonstrate secretory cells in the normal FT, a selected section is depicted for PAX8 and DIO3 images. 20X magnification, scale bars: 20 μm **(B)** IF staining for PAX8 and DIO3 in normal FT epithelium (10X magnification, scale bars: 10 μm) and for nucleus (Hoechst) and DIO3 in STIC and HGSOC tumor areas (20X magnification, scale bars: 20 μm) **(C)** IHC staining of PAX8 and DIO3 in a representative BRCA1/p53/PTEN ovarian cancer mouse tissue. 20X magnification, scale bars: 20 μm.

significant protein-protein interaction (PPI) enrichment p-value (<8.09e-10), confirms that this group is biologically connected. A selected set of 55 proteins was divided to three subcategories of biological processes (Table 1). The first group consists proteins involved in thyroid hormone mediated signaling [33–36], including the nuclear receptor-binding SET domain-containing protein 1 (NSD1), thyroid receptor-interacting protein 11 (TRIP11) and Cathepsin L (CTSL). The elevation observed in these proteins corresponds with our demonstration of increased T3 bioavailability in the DIO3-KD cells. The second major group is associated with metabolism and includes an elevation in the mitochondrial ATP synthase complex, which facilitates oxidative phosphorylation [32]. In parallel, two central glycolysis proteins, GAPDH and Hexokinase 1 (HK1), were significantly reduced, although below the 25% cut-off. Notably, the changes in GAPDH and ATP5A levels were also evident by WB (Fig. 3I). These results support our observation of an attenuated Warburg effect in the DIO3-depleted cells and are in accord with the known role of T3 in promoting mitochondrial respiration. Another major pathway controlling cell metabolism is autophagy. A central autophagy related protein, MAPILC3B, shown to induce ovarian cancer cell migration, adhesion and invasion [37], was significantly reduced in our DIO3-KD cells. The third group includes proteins facilitating tumor growth and suppression. For example, Ribonuclease T2 (RNASET2), shown to inhibit ovarian cancer growth *in vivo* [38], was completely absent in the control cells and uniquely expressed in the DIO3 silenced cells. In addition, proteins which trigger apoptosis, such as Histidine triad nucleotide-binding protein 1 (HINT1)

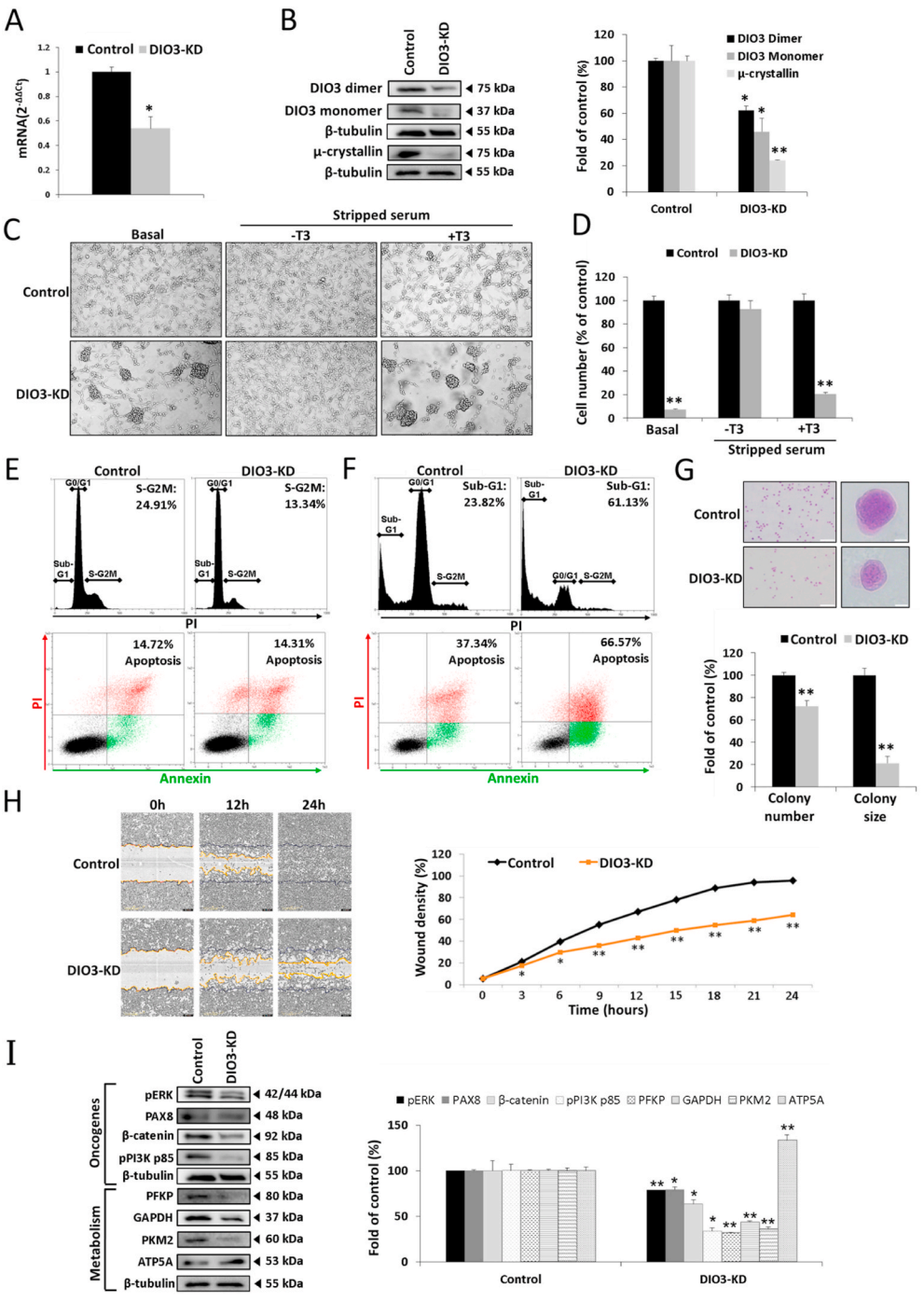

Fig. 3. DIO3 silencing in HGSOC cells displays T3-related anti-cancer effects. Isolated clones of control and DIO3-KD cells were examined for **(A)** DIO3 mRNA levels by real-time PCR **(B)** DIO3 and μ-crystallin protein levels by WB (Left panel). β-tubulin was used as loading control. Quantification of normalized bands intensity as fold of control is presented in the right panel. Values are mean ± STE. *, $p < 0.05$. **,$p < 0.005$ **(C)** Microscopy images (10X objective) of cells seeded (0.5×10^6/25 mm flasks) either in full medium (Left panel) or in medium with charcoal-stripped serum, containing depleted levels of thyroid hormones (Middle panel). After 11 days in culture, cells grown in the charcoal-stripped serum were supplemented with 1 nM T3 for 1 week (Right panel) **(D)** Cell counts, quantified using NIH ImageJ software. Experiments were independently repeated three times. Flow cytometry analyses of cell cycle and apoptosis (Annexin+/PI− and Annexin+/PI+) for cells grown **(E)** 3 days in culture **(F)** a week in culture. Percentage of S-G2M, Sub-G1 and apoptosis are shown. Experiments were independently repeated at least twice. **(G)** Representative image of soft agar colony formation assay (Upper panel). Left images- 10X objective, scale bars: 100 μm. Right images- 20X objective, scale bars: 10 μm. Colony number and size as fold of control (Lower panel). Values are mean ± STE, **, $p < 0.005$. Results were repeated in four replicates **(H)** Representative images of wound healing closure in the cells (4×10^4/96 well plates) for up to 24 h using the IncuCyte ZOOM™ real time live cell imaging system. Blue lines depict scratch baseline and orange lines closure area. Graph of the relative wound density over time is shown on the right panel. Values are mean ± STE, *, $p < 0.05$. **,$p < 0.005$. Experiments were independently repeated twice in triplicates **(I)** Cells were analyzed by WB for a collection of proteins involved in oncogenic signaling pathways and glucose metabolism. β-tubulin was used as loading control. Quantification of normalized bands intensity as fold of control is presented in the right panel. Values are mean ± STE, *, $p < 0.05$. **,$p < 0.005$. All WB's are representative of at least two independent repeats. (For interpretation of the references to colour in this figure legend, the reader is referred to the Web version of this article.)

[39] and Cathepsin C (CTSC) [40], were elevated. Collectively, these alterations in an array of cancer-relevant proteins support our observations of DIO3 involvement in HGSOC cell proliferation, apoptosis, and metabolic reprogramming.

4. Discussion

Here we demonstrate the expression and functional role of DIO3, the T3-catabolizing enzyme, in HGSOC. This protein was evident in its homodimeric conformation, which is highly stable and indicates activity [23,24]. DIO3 was highly expressed in premalignant lesion of HGSOC, known as STIC, as well as in primary and metastatic tissues. In normal tissues, ovaries were DIO3 negative, while secretory cells of the fallopian tube, which are considered the cell–of-origin for HGSOC, were positive. This expression pattern in normal and malignant cells corresponds with that of the Müllerian marker PAX8 [3]. Additional studies, however, are needed to clarify whether similar to PAX8 [41] DIO3 has little functional effect in fully differentiated fallopian tube. Collectively, we demonstrated that DIO3 is maintained throughout tumor evolution, from normal to transformed cells.

We further established a functional link between DIO3 regulation of T3 and HGSOC tumorigenesis, an association which was demonstrated thus far in few malignancies [10–14]. Stable depletion of DIO3 in HGSOC cells, attenuated several hallmarks of carcinogenesis including cell proliferation, migration and anchorage-independent growth as well as induced apoptosis. The latter was supported by proteomics analysis

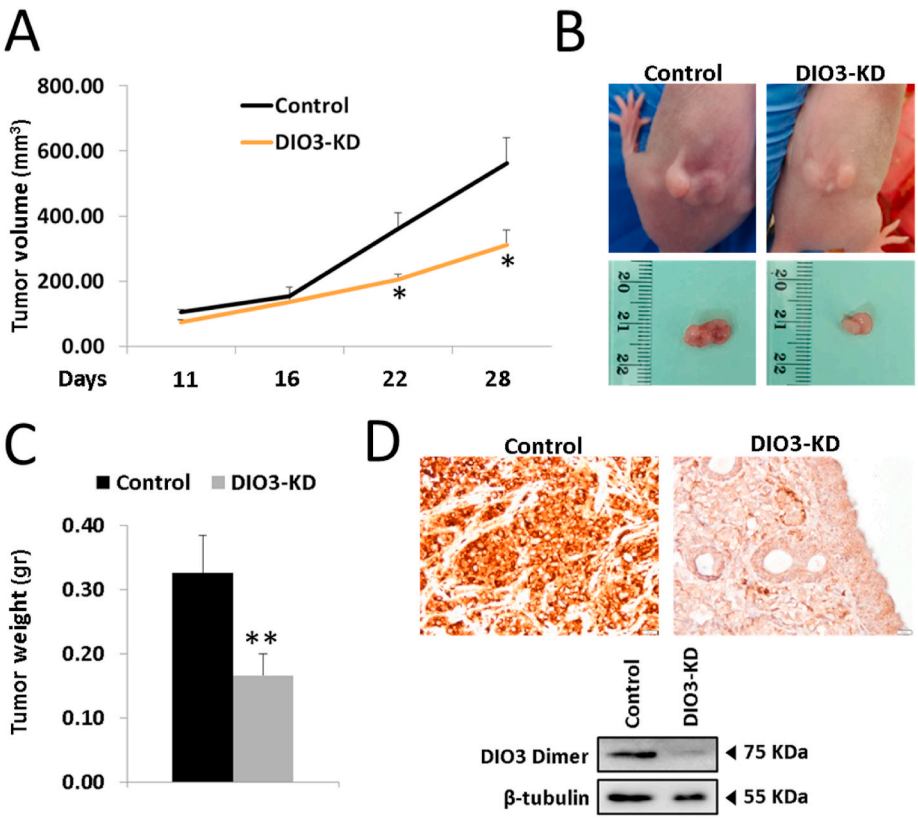

Fig. 4. DIO3 silencing attenuates HGSOC tumor growth in nude mice (A) Average tumor volume over the study period in mice (n = 7) inoculated with control (Left flank) and DIO3-KD cells (Right flank). Values are mean ± STE, *, $p < 0.05$ **(B)** Representative mouse and excised tumors at study end. Left panel depicts control tumors and the right panel DIO3-KD tumors **(C)** Average tumor weight at study end. Values are mean ± STE, **, $p < 0.005$ **(D)** DIO3 expression in representative control and DIO3-KD tumors by IHC (Upper panel, 20X magnification, scale bars: 20 μm) and WB (Lower panel, β-tubulin used as loading control).

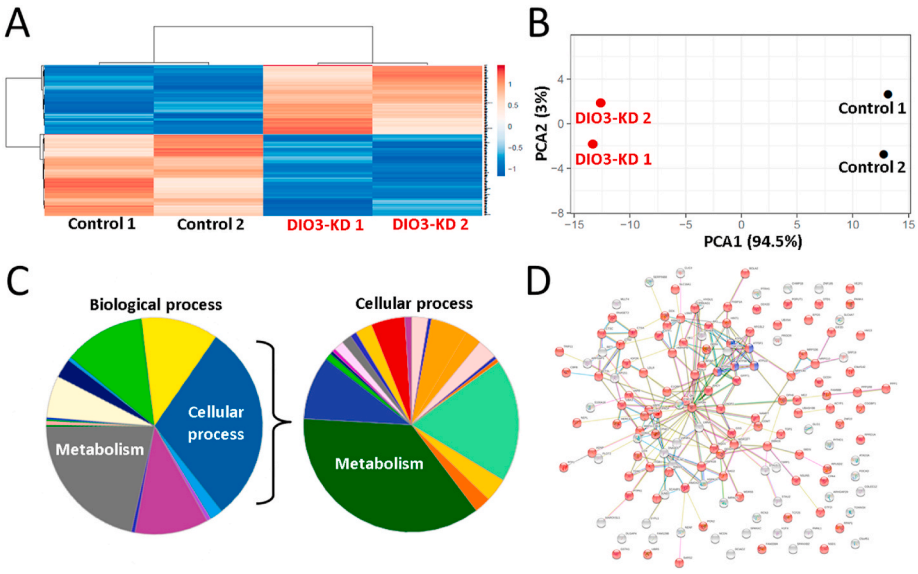

Fig. 5. DIO3-silencing in HGSOC leads to alterations in an array of cancer and metabolic relevant proteins. Proteomics results of control (control 1, control 2) and DIO3-KD (DIO3-KD 1, DIO3-KD 2) duplicates were analyzed by **(A)** Unsupervised hierarchical protein clustering (ClustVis tool). Unit variance scaling is applied to rows. Both rows and columns are clustered using correlation distance and average linkage **(B)** Principal component analysis (PCA) by ClustVis tool. Unit variance scaling is applied to rows, singular value decomposition (SVD) were used to calculate principle components. X axis shows principle component 1 that explain 94.5% of the total variance and Y axis shows principle component 2 that explain 3% of the total variance **(C)** Pie charts results (PANTHER tool) analyzing biological and cellular processes. The main subcategories are depicted **(D)** Interaction network of proteins altered between control and DIO3-KD cells (STRING tool). Proteins associated with metabolism are marked in red. The original full-size image is presented in Supplementary Fig. 5. (For interpretation of the references to colour in this figure legend, the reader is referred to the Web version of this article.)

identifying an elevation in several pro-apoptotic proteins and is in accordance with previous studies in cancer models demonstrating T3 involvement in cell death [42–44]. Mice xenografts inoculated with the DIO3-silenced cells, presented a similar growth inhibition. This phenotype is supported by a significant reduction in an array of oncogenic pathways relevant to ovarian cancer growth, including pERK, β-catenin and PI3K. PAX8, a lineage-specific transcription factor which contributes to HGSOC proliferation [41,45], was also reduced. Additional reinforcement was provided by proteomics analysis, indicating elevation in several tumor suppressors. These include RNASET2, shown to inhibit ovarian cancer growth *in vivo* [38] and MARCKSL1 which exhibited anti-angiogenic effects in ovarian tumors [46]. Taken together, our *in vitro* and *in vivo* results confirmed that HGSOC is DIO3-addicted. We further demonstrated that this dependence on DIO3 is T3-mediated. This corresponds with attenuated degradation and increased biological activity of T3 in DIO3-silenced cells. Accordingly, in our DIO3-KD cells we observed alterations in several proteins known to directly regulate T3 bioavailability. These include a reduction in

Table 1
Proteomics analysis of selected proteins altered in DIO3-KD HGSOC cells.

Gene	Description	% change	p-value	
NSD1	Nuclear Receptor Binding SET Domain Protein 1	601%	0.045	**Thyroid hormone related**
TRIP11	Thyroid Hormone Receptor Interactor 11	228%	0.008	
CTSL	Cathepsin L	101%	0.026	
ATP5PB	ATP Synthase Peripheral Stalk-Membrane Subunit b	58%	0.032	**Metabolism**
ATP5B	ATP Synthase Subunit Beta	41%	0.022	
ATP5A1	ATP Synthase Subunit Alpha	38%	0.001	
ATP5O	ATP Synthase Peripheral Stalk Subunit OSCP	36%	0.018	
ATP5J2	ATP synthase membrane subunit f	25%	0.016	
SARS2	Seryl-TRNA Synthetase 2, Mitochondrial	Unique	0.001	
ME2	Malic Enzyme 2	105%	0.008	
GCDH	Glutaryl-CoA Dehydrogenase	73%	0.048	
PANK4	Pantothenate Kinase 4	54%	0.013	
SLC16A1	Solute Carrier Family 16 Member 1	47%	0.001	
PRKAG1	Protein Kinase AMP-Activated Non-Catalytic Subunit γ 1	42%	0.004	
AFG3L2	AFG3 Like Matrix AAA Peptidase Subunit 2	29%	0.025	
ACAD9	Acyl-CoA Dehydrogenase Family Member 9	22%	0.035	
NAMPT	Nicotinamide Phosphoribosyltransferase	−54%	0.042	
TOMM34	Translocase Of Outer Mitochondrial Membrane 34	−53%	0.005	
MAP1LC3B	Microtubule Associated Protein 1 Light Chain 3 Beta	−43%	0.046	
RHEB	Ras Homolog, MTORC1 Binding. GTP-Binding Protein Rheb	−42%	0.044	
ATAD3A	ATPase Family AAA Domain Containing 3A	−26%	0.027	
NQO1	NAD(P)H Quinone Dehydrogenase 1	−26%	0.009	
GFPT1	Glutamine-fructose-6-phosphate aminotransferase 1	−26%	0.047	
PYGB	Glycogen Phosphorylase B	−24%	0.032	
IDH3B	Isocitrate Dehydrogenase (NAD(+)) 3 Non-Catalytic Subunit β	−23%	0.013	
GAPDH	Glyceraldehyde-3-Phosphate Dehydrogenase	−16%	0.006	
HK1	Hexokinase 1	−12%	0.050	
RNASET2	Ribonuclease T2	Unique	0.022	**Tumor growth and suppression**
MARCKSL1	MARCKS Like 1	48%	0.019	
IGF2R	Insulin Like Growth Factor 2 Receptor	316%	0.017	
RPRD1A	Regulation Of Nuclear Pre-MRNA Domain Containing 1A	111%	0.039	
AFDN	Afadin, Adherens Junction Formation Factor	72%	0.049	
CLIC4	Chloride Intracellular Channel 4	65%	0.033	
CNDP2	Carnosine Dipeptidase 2	58%	0.022	
TCF25	Transcription Factor 25	55%	0.004	
UBA1	Ubiquitin Like Modifier Activating Enzyme 1	55%	0.033	
OCIAD2	Ovarian Cancer Immunoreactive Antigen Domain Containing 2	38%	0.003	
C1QBP	Complement C1q Binding Protein	38%	0.016	
UBR5	Ubiquitin Protein Ligase E3 Component *N*-Recognin 5	36%	0.026	
HERC4	HECT And RLD Domain Containing E3 Ubiquitin Protein Ligase 4	36%	0.033	
S100A16	S100 Calcium Binding Protein A16	32%	0.036	
CTSC	Cathepsin C	31%	0.043	
HINT1	Histidine Triad Nucleotide Binding Protein 1	30%	0.007	
VEZF1	Vascular Endothelial Zinc Finger 1	26%	0.037	
RAD21	RAD21 Cohesin Complex Component	26%	0.010	
PAXX	PAXX Non-Homologous End Joining Factor	−100%	0.013	
RNF114	Ring Finger Protein 114	−63%	0.015	
CBFB	Core-Binding Factor Subunit Beta	−57%	0.030	
SBDS	SBDS Ribosome Maturation Factor	−40%	0.022	
CSE1L	Chromosome Segregation 1 Like, Exportin-2	−35%	0.048	
TOP1	DNA Topoisomerase I	−34%	0.037	
FLNC	Filamin C	−31%	0.012	
HSPB1	Heat Shock Protein Family B (Small) Member 1	−29%	0.0002	
HSPA1A	Heat Shock Protein Family A (Hsp70) Member 1A	−25%	0.014	
LOX	Lysyl Oxidase	−25%	0.046	

Unique, protein identified exclusively in the DIO3-KD cells.

μ-crystallin, a cytosolic enzyme which binds and augments T3-mediated gene expression [28,29]. Notably, T3 was shown to inhibit the activity of this enzyme [30], suggesting a reciprocal relationship between thyroid hormone bioavailability and μ-crystallin activity. In parallel, upregulation was documented in TRIP11 which localizes to the nucleus and enhances T3-dependent transcription [33] and NSD1, which was shown to bind nuclear thyroid receptor [34]. CTSL was also elevated and is known to liberate thyroid hormone from its binding protein and to suppress ovarian cancer progression [35,36]. These collective results indicate that depletion of DIO3 in HGSOC cells leads to the stimulation of T3 bioavailability.

Cancer is characterized by metabolic reprogramming, in which the cells predominantly utilize glycolysis for ATP production, even when oxygen is available. This process is known as aerobic glycolysis, or the Warburg effect [4,47]. In that regard, T3 attenuates aerobic glycolysis via promotion of mitochondrial energy production [5]. This emphasizes why cancer cells facilitate T3 inactivation by expressing the DIO3 enzyme, to enhance the Warburg effect [8]. Consequently, following DIO3 silencing we observed a reduction in key glycolysis players, including GAPDH and PKM2. The latter, a vital driver of the Warburg effect [31], was shown to bind T3 which in turn allosterically inhibits PKM2 activity [48].

On the other hand, we observed induction in mitochondrial subunits of the ATP5 complex, which synthesizes ATP from ADP as part of the oxidative phosphorylation [32]. Notably, a positive correlation between T3 and the ATP5 complex was previously reported in the ovaries [49].

To conclude, in this work we established the pivotal role of DIO3 in facilitating ovarian cancer growth and metabolic reprogramming, via

dynamic depletion of intracellular T3. This proposes that inhibiting DIO3 may serve as an utterly original approach to rewire mitochondrial energy and attenuate tumor growth.

Authors' contributions

D.M preformed, analyzed and interpreted the experimental data. A.A and Y·F performed some of the methods. A.W, A.K, D. K assisted in the IHC assays and D. K and E.E analyzed the IHC slides. D. V and R.P provided the cancer mouse tissues. N.A, Y·K and A.F assisted in Human tissues collection. B.L assisted in study design. O.A.F. designed, analyzed and interpreted the experimental data. D. M, M.E. and O.A.F. wrote the manuscript. All authors read and approved the manuscript.

Declaration of competing interest

The authors declare that they have no known competing financial interests or personal relationships that could have appeared to influence the work reported in this paper.

Acknowledgements

The work of Dotan Moskovich was done in partial fulfillment of the requirements for a PhD degree from the Sackler Faculty of Medicine, Tel Aviv University, Israel. O.A.F and B.L received support from the Israel Innovation Authority, Nofar Program for Applied Research in Academia, Ministry of Economics (Project 59435).

Appendix A. Supplementary data

Supplementary data to this article can be found online at https://doi.org/10.1016/j.canlet.2020.11.011.

References

[1] G.C. Jayson, E.C. Kohn, H.C. Kitchener, J.A. Ledermann, Ovarian cancer, Lancet 384 (2014) 1376–1388.
[2] S.I. Labidi-Galy, E. Papp, D. Hallberg, N. Niknafs, V. Adleff, M. Noe, R. Bhattacharya, M. Novak, S. Jones, J. Phallen, High grade serous ovarian carcinomas originate in the fallopian tube, Nat. Commun. 8 (2017) 1093.
[3] R. Perets, R. Drapkin, It's totally tubular riding the new wave of ovarian cancer research, Canc. Res. 76 (2016) 10–17.
[4] M.G. Vander Heiden, L.C. Cantley, C.B. Thompson, Understanding the Warburg effect: the metabolic requirements of cell proliferation, Science 324 (2009) 1029–1033.
[5] I.M. Goemann, M. Romitti, E.L.S. Meyer, S.M. Wajner, A.L. Maia, Role of thyroid hormones in the neoplastic process: an overview, Endocr. Relat. Canc. 24 (2017) R367–R385.
[6] A. Sibilio, R. Ambrosio, C. Bonelli, M. De Stefano, V. Torre, M. Dentice, D. Salvatore, Deiodination in cancer growth: the role of type III deiodinase, Minerva Endocrinol. 37 (2012) 315–327.
[7] C. Luongo, M. Dentice, D. Salvatore, Deiodinases and their intricate role in thyroid hormone homeostasis, Nat. Rev. Endocrinol. 15 (2019) 479–488.
[8] D. Ciavardelli, M. Bellomo, C. Crescimanno, V. Vella, Type 3 deiodinase: role in cancer growth, stemness, and metabolism, Front. Endocrinol. 5 (2014) 215.
[9] I.M. Goemann, V.R. Marczyk, M. Romitti, S.M. Wajner, A.L. Maia, Current concepts and challenges to unravel the role of iodothyronine deiodinases in human neoplasias, Endocr. Relat. Canc. 25 (2018) R625–R645.
[10] D. Di Girolamo, R. Ambrosio, M.A. De Stefano, G. Mancino, T. Porcelli, C. Luongo, E. Di Cicco, G. Scalia, L. Del Vecchio, A. Colao, Reciprocal interplay between thyroid hormone and microRNA-21 regulates hedgehog pathway–driven skin tumorigenesis, J. Clin. Invest. 126 (2016) 2308–2320.
[11] V. Catalano, M. Dentice, R. Ambrosio, C. Luongo, R. Carollo, A. Benfante, M. Todaro, G. Stassi, D. Salvatore, Activated thyroid hormone promotes differentiation and chemotherapeutic sensitization of colorectal cancer stem cells by regulating Wnt and BMP4 signaling, Canc. Res. 76 (2016) 1237–1244.
[12] M. Romitti, S.M. Wajner, L. Ceolin, C.V. Ferreira, R. Ribeiro, H.C. Rohenkohl, L. P. Weber SdeS, C. Fuziwara, E. Kimura, A. Maia, MAPK and SHH pathways modulate type 3 deiodinase expression in papillary thyroid carcinoma, Endocr. Relat. Canc. 23 (2016) 135–146.
[13] M. Dentice, C. Luongo, R. Ambrosio, A. Sibilio, A. Casillo, A. Iaccarino, G. Troncone, G. Fenzi, P.R. Larsen, D. Salvatore, beta-Catenin regulates deiodinase levels and thyroid hormone signaling in colon cancer cells, Gastroenterology 143 (2012) 1037–1047.
[14] M. Dentice, C. Luongo, S. Huang, R. Ambrosio, A. Elefante, D. Mirebeau-Prunier, A. M. Zavacki, G. Fenzi, M. Grachtchouk, M. Hutchin, Sonic hedgehog-induced type 3 deiodinase blocks thyroid hormone action enhancing proliferation of normal and malignant keratinocytes, Proc. Natl. Acad. Sci. Unit. States Am. 104 (2007) 14466–14471.
[15] R. Perets, G.A. Wyant, K.W. Muto, J.G. Bijron, B.B. Poole, K.T. Chin, J.Y.H. Chen, A.W. Ohman, C.D. Stepule, S. Kwak, Transformation of the fallopian tube secretory epithelium leads to high-grade serous ovarian cancer in Brca; Tp53; Pten models, Canc. Cell 24 (2013) 751–765.
[16] E. Shinderman-Maman, K. Cohen, C. Weingarten, D. Nabriski, O. Twito, L. Baraf, A. Hercbergs, P.J. Davis, H. Werner, M. Ellis, O. Ashur-Fabian, The thyroid hormone-alphavbeta3 integrin axis in ovarian cancer: regulation of gene transcription and MAPK-dependent proliferation, Oncogene 35 (2016) 1977–1987.
[17] K. Cohen, M. Ellis, S. Khoury, P.J. Davis, A. Hercbergs, O. Ashur-Fabian, Thyroid hormone is a MAPK-dependent growth factor for human myeloma cells acting via alphavbeta3 integrin, Mol. Canc. Res. 9 (2011) 1385–1394.
[18] T. Metsalu, J. Vilo, ClustVis: a web tool for visualizing clustering of multivariate data using Principal Component Analysis and heatmap, Nucleic Acids Res. 43 (2015) W566–W570.
[19] H. Mi, A. Muruganujan, X. Huang, D. Ebert, C. Mills, X. Guo, P.D. Thomas, Protocol Update for large-scale genome and gene function analysis with the PANTHER classification system (v. 14.0), Nat. Protoc. 14 (2019) 703–721.
[20] D. Szklarczyk, J.H. Morris, H. Cook, M. Kuhn, S. Wyder, M. Simonovic, A. Santos, N.T. Doncheva, A. Roth, P. Bork, The STRING database in 2017: quality-controlled protein–protein association networks, made broadly accessible, Nucleic Acids Res. (2016), gkw937.
[21] S. Domcke, R. Sinha, D.A. Levine, C. Sander, N. Schultz, Evaluating cell lines as tumour models by comparison of genomic profiles, Nat. Commun. 4 (2013) 2126.
[22] A.M. Karst, R. Drapkin, Primary culture and immortalization of human fallopian tube secretory epithelial cells, Nat. Protoc. 7 (2012) 1755.
[23] U. Schweizer, C. Schlicker, D. Braun, J. Köhrle, C. Steegborn, Crystal structure of mammalian selenocysteine-dependent iodothyronine deiodinase suggests a peroxiredoxin-like catalytic mechanism, Proc. Natl. Acad. Sci. Unit. States Am. 111 (2014) 10526–10531.
[24] G.V. Sagar, B. Gereben, I. Callebaut, J.-P. Mornon, A. Zeöld, C. Curcio-Morelli, J. W. Harney, C. Luongo, M.A. Mulcahey, P.R. Larsen, The thyroid hormone-inactivating deiodinase functions as a homodimer, Mol. Endocrinol. 22 (2008) 1382–1393.
[25] C. Curcio-Morelli, B. Gereben, A.M. Zavacki, B.W. Kim, S. Huang, J.W. Harney, P. R. Larsen, A.C. Bianco, In vivo dimerization of types 1, 2, and 3 iodothyronine selenodeiodinases, Endocrinology 144 (2003) 937–946.
[26] F. Santini, I.J. Chopra, D.H. Solomon, G. Chua Teco, Evidence that the human placental 5-monodeiodinase is a phospholipid-requiring enzyme, J. Clin. Endocrinol. Metab. 74 (1992) 1366–1371.
[27] K. Visvanathan, R. Vang, P. Shaw, A. Gross, R. Soslow, V. Parkash, I.-M. Shih, R. J. Kurman, Diagnosis of serous tubal intraepithelial carcinoma based on morphologic and immunohistochemical features: a reproducibility study, Am. J. Surg. Pathol. 35 (2011) 1766.
[28] K. Takeshige, T. Sekido, J.-i. Kitahara, Y. Ohkubo, D. Hiwatashi, H. Ishii, S.-i. Nishio, T. Takeda, M. Komatsu, S. Suzuki, Cytosolic T3-binding protein modulates dynamic alteration of T3-mediated gene expression in cells, Endocr. J. 61 (2014) 561–570.
[29] D. Seko, S. Ogawa, T.-S. Li, A. Taimura, Y. Ono, μ-Crystallin controls muscle function through thyroid hormone action, Faseb. J. 30 (2016) 1733–1740.
[30] A. Hallen, A.J. Cooper, J.F. Jamie, P.A. Haynes, R.D. Willows, Mammalian forebrain ketimine reductase identified as μ-crystallin; potential regulation by thyroid hormones, J. Neurochem. 118 (2011) 379–387.
[31] L.B. Tanner, A.G. Goglia, M.H. Wei, T. Sehgal, L.R. Parsons, J.O. Park, E. White, J. E. Toettcher, J.D. Rabinowitz, Four key steps control glycolytic flux in mammalian cells, Cell systems 7 (2018) 49–62, e48.
[32] A.I. Jonckheere, J.A. Smeitink, R.J. Rodenburg, Mitochondrial ATP synthase: architecture, function and pathology, J. Inherit. Metab. Dis. 35 (2012) 211–225.
[33] Y. Chen, P.-L. Chen, C.-F. Chen, Z.D. Sharp, W.-H. Lee, Thyroid hormone, T3-dependent phosphorylation and translocation of Trip230 from the Golgi complex to the nucleus, Proc. Natl. Acad. Sci. Unit. States Am. 96 (1999) 4443–4448.
[34] N. Huang, E. vom Baur, J.M. Garnier, T. Lerouge, J.L. Vonesch, Y. Lutz, P. Chambon, R. Losson, Two distinct nuclear receptor interaction domains in NSD1, a novel SET protein that exhibits characteristics of both corepressors and coactivators, EMBO J. 17 (1998) 3398–3412.
[35] B. Friedrichs, C. Tepel, T. Reinheckel, J. Deussing, K. von Figura, V. Herzog, C. Peters, P. Saftig, K. Brix, Thyroid functions of mouse cathepsins B, K, and L, J. Clin. Invest. 111 (2003) 1733–1745.
[36] L. Zhang, L. Wei, G. Shen, B. He, W. Gong, N. Min, L. Zhang, Y. Duan, J. Xie, H. Luo, Cathepsin L is involved in proliferation and invasion of ovarian cancer cells, Mol. Med. Rep. 11 (2015) 468–474.
[37] Z. Tang, N. Zhang, W. Di, W. Li, Inhibition of microtubule-associated protein 1 light chain 3B via small-interfering RNA or 3-methyladenine impairs hypoxia-induced HO8910PM and HO8910 epithelial ovarian cancer cell migration and invasion and is associated with RhoA and alterations of the actin cytoskeleton, Oncol. Rep. 33 (2015) 1411–1417.
[38] F. Acquati, S. Bertilaccio, A. Grimaldi, L. Monti, R. Cinquetti, P. Bonetti, M. Lualdi, L. Vidalino, M. Fabbri, M.G. Sacco, Microenvironmental control of malignancy exerted by RNASET2, a widely conserved extracellular RNase, Proc. Natl. Acad. Sci. Unit. States Am. 108 (2011) 1104–1109.
[39] J. Weiske, O. Huber, The histidine triad protein Hint1 triggers apoptosis independent of its enzymatic activity, J. Biol. Chem. 281 (2006) 27356–27366.

[40] M. Mrschtik, K.M. Ryan, Lysosomal proteins in cell death and autophagy, FEBS J. 282 (2015) 1858–1870.
[41] L.H. Rodgers, Ó. Eoghainín, J.E. Burdette, Loss of PAX8 in high-grade serous ovarian cancer reduces cell survival despite unique modes of action in the fallopian tube and ovarian surface epithelium, Oncotarget 7 (2016) 32785.
[42] C. Luongo, R. Ambrosio, S. Salzano, A.A. Dlugosz, C. Missero, M. Dentice, The sonic hedgehog-induced type 3 deiodinase facilitates tumorigenesis of basal cell carcinoma by reducing Gli2 inactivation, Endocrinology 155 (2014) 2077–2088.
[43] P. Sar, R. Peter, B. Rath, A.D. Mohapatra, S.K. Mishra, 3, 3′ 5 triiodo L thyronine induces apoptosis in human breast cancer MCF-7cells, repressing SMP30 expression through negative thyroid response elements, PloS One 6 (2011), e20861.
[44] M. Hara, S. Suzuki, J.-i. Mori, K. Yamashita, M. Kumagai, T. Sakuma, T. Kakizawa, T. Takeda, T. Miyamoto, K. Ichikawa, Thyroid hormone regulation of apoptosis induced by retinoic acid in promyeloleukemic HL-60 cells: studies with retinoic acid receptor-specific and retinoid× receptor-specific ligands, Thyroid 10 (2000) 1023–1034.
[45] D. Ghannam-Shahbari, E. Jacob, R.R. Kakun, T. Wasserman, L. Korsensky, O. Sternfeld, J. Kagan, D.R. Bublik, S. Aviel-Ronen, K. Levanon, PAX8 activates a p53-p21-dependent pro-proliferative effect in high grade serous ovarian carcinoma, Oncogene (2018) 1.
[46] B.-R. Kim, S.-H. Lee, M.-S. Park, S.-H. Seo, Y.-M. Park, Y.-J. Kwon, S.-B. Rho, MARCKSL1 exhibits anti-angiogenic effects through suppression of VEGFR-2-dependent Akt/PDK-1/mTOR phosphorylation, Oncol. Rep. 35 (2016) 1041–1048.
[47] P.S. Ward, C.B. Thompson, Metabolic reprogramming: a cancer hallmark even warburg did not anticipate, Canc. Cell 21 (2012) 297–308.
[48] S. Cheng, J. Leonard, P. Davis, Molecular aspects of thyroid hormone actions, Endocr. Rev. 31 (2010) 139–170.
[49] M. Colella, D. Cuomo, A. Giacco, M. Mallardo, M. De Felice, C. Ambrosino, Thyroid hormones and functional ovarian reserve: systemic vs. Peripheral dysfunctions, J. Clin. Med. 9 (2020) 1679.